EFFECTS OF CELL SIZE AND CELL WALL THICKNESS VARIATIONS ON THE STRENGTH OF CLOSED-CELL FOAMS USING LAGUERRE TESSELLATION

Youming Chen[1, 2], Raj Das[2, 3] and Mark Battley[2]

[1] School of Automotive Engineering, Wuhan University of Technology, Wuhan, Hubei Province, China, Email: cyou659@aucklanduni.ac.nz
[2] Centre for Advanced Composite Materials, Department of Mechanical Engineering, The University of Auckland, Auckland, New Zealand, Email: m.battley@auckland.ac.nz
[3] Sir Lawrence Wackett Aerospace Research Centre, School of Engineering, RMIT University, GPO Box 2476, Melbourne, VIC 3001, Australia, Email: raj.das@rmit.edu.au

Keywords: Closed-cell foam; Laguerre tessellation; Cell size; Cell wall thickness; Strength

ABSTRACT

In this work, the effects of cell size and cell wall thickness variations on the compressive and shear strengths of closed-cell foams were investigated using Laguerre tessellation models. It is found that the compressive and shear strengths of closed-cell foams decrease as cell size and cell wall thickness variations increase, and the compressive strength reduces more significantly. At a given level of variation, the effect of cell size variation on strength reduction is comparable to that of cell wall thickness variation on them. In the foam studied (M130 foam), cell wall thickness has a larger dispersion than cell size, and therefore is the main contributor to the strength reduction of the foam. In comparison to compressive and shear stiffnesses, cell size and cell wall thickness variations reduce compressive and shear strengths more significantly.

1 INTRODUCTION

Foam materials are used in a large number of applications including packaging, heat insulation, acoustic isolation, impact absorber, cores of sandwich structures, filters and flotation, due to their property advantages such as lightweight, high impact absorption and acoustic attenuation, and low thermal conductivity [1]. In these applications, especially for sandwich cores and impact energy absorbers, the mechanical performance of foams is critical. Study on foam mechanics could help not only engineers to use foams safely and efficiently, but also manufacturers to improve the mechanical properties of foams.

It is well recognised that the global properties of foams are dependent on the properties of materials from which the foams are made (base materials) and foam microstructures. Experimental study on the property-microstructure relationship of foams is limited, because foams with prescribed microstructures are difficult to manufacture. Micromechanical modelling is a technique which predicts the macroscopic properties of heterogeneous materials based on the properties of constituent materials and their microstructures. It is well-suited for investigating the property-microstructure of foams, and many foam micro-models have been developed over the last decades [1-34], which basically fall into three categories: space-filling polyhedron [1, 13, 14], tessellation-based [7-11, 15-20] and image-based models [21-34].

Space-filling polyhedron models simplify foam cells as a single polyhedron. The widely-used space-filling polyhedron models include the cubic model [1], Kelvin model [13] and Weaire-Phelan model [14]. These models have simple geometry, and thus can be readily constructed and analysed using the classic beam and shell theory. Finite element models can be directly developed from computed tomography images by turning voxels representing solid phases into solid elements [27, 29, 31, 35-37], termed image-based models. The key advantage of image-based foam models is that these models have the same geometry as the scanned foam specimens. Because of this, these are well-suited to exploring the deformation and failure mechanisms at cell level in foams [21, 24, 29, 31-34].

However, apart from being computationally expensive [29, 31, 35], the geometry of image-based models is determined by the scanned foam specimens and cannot be generated arbitrarily with various user specified microstructures, which make them unsuitable for investigating foam properties-microstructure relationship.

Random tessellations including Voronoi tessellation [7-9, 15-17] and Laguerre tessellation models [10, 11] are often adopted to model foams. This is because the processes of generating these tessellations resemble the actual processes of foam formation. Moreover, Voronoi and Laguerre tessellations can be created such that the cell geometry complies with Matzke's observation [38]. For example, Voronoi tessellations based on random sequential adsorption algorithm and random close packing algorithm have an average number of faces per cell of 14.9 and 14.2, respectively [9, 39]. Laguerre tessellations constructed through random closely packing spheres have the average number of faces per cell ranging from 14.11 to 13.04 and the average number of edges per face ranging from 5.14 to 5.09 [11, 40-42]. Additionally, Laguerre tessellations can be produced with cell volume following a prescribed distribution, which makes it more effective than Voronoi tessellations in foam modelling [10, 11, 18-20]. Last but not least, tessellation-based models can be discretised by shell elements, and thus are computationally efficient. As tessellation-based models are capable of incorporating foam microstructural variability and imperfections, such as irregularity [7, 9, 17, 43, 44], cell size variation [10, 11], cell wall thickness variation [10], cell wall curvature [9], and missing cell faces [45], these models are often adopted to investigate the effects of these on the macroscopic properties of foams.

The compressive strength of closed-cell foams has been studied using the Kelvin model in [2, 46, 47]. But, it was reported that the strengths of real foams are much lower than that of the Kelvin foam [48, 49]. Hence, numerical models which are integrated with more realistic microstructural characteristics are needed for closed-cell foams in order to accurately predict their strength. The variability in cell size and cell wall thickness is ubiquitous in real foams. The influences of these variations on the stiffness of closed-cell foams have been investigated in [4, 10, 11, 50]. However, the effects of these variations on the strength of closed-cell foams have not been investigated. Additionally, when used as sandwich cores, foams are primarily subjected to shear loads, and thus the shear response of foams is of significant concern for designers. Nevertheless, numerical modelling mostly focuses on the compressive response of foams so far. Modelling of the nonlinear elastic-plastic shear response of foams has not been reported. In our previous study [10], the effect on cell size and cell wall thickness variations on the stiffness of closed-cell foams were investigated using Laguerre tessellations models. In the present study, the nonlinear compressive and shear responses of closed-cell foams are studied using the Laguerre tessellation models previously developed in [10], and the effects of cell size and cell wall thickness variations on the compressive and shear strengths of closed-cell foams are explored.

2 MATERIAL PROPERTIES

The foam studied in this work is commercial polymeric closed foam with a trade name M130 (from Gurit Ltd.) which is widely used in the marine industry. M130 foam is made of styrene–acrylonitrile (SAN). The density and strengths of the foam from the datasheet [51] and experiments [52] are listed in Table 1. The base material of the foam is treated as elastic-perfectly plastic and Table 1 provides the properties of the base material of the foam used here. The measurements of cell size and wall thickness and the generation of Laguerre tessellation models incorporating measured relative density, cell size and cell wall thickness distributions can be found in the previous work of the present authors [10]. The measured cells sizes have an average of 418 μm and a standard deviation of 140 μm, and the measured cell wall thicknesses have an average of 18.9 μm and a standard deviation of 18.1 μm.

Properties	Datasheet (Gurit Ltd.) [51]	Experimental results [52]
Density (kg/m3)	140 ± 10	148 ± 3.7
Relative density	(0.1308± 0.009)	(0.1383 ± 0.003)
Compressive strength (MPa) (Standard)	2.31 (ASTMD1621)	3.15 (ISO 844)
Shear strength (MPa) (Standard)	1.98 (ASTMC273)	2.27 (ASTMC273)

Table 1: Properties of M130 foam from the datasheet and experiment.

Density	Young's modulus	Yield strength	Poisson's ratio
1070 kg/m3 [53]	3.58 GPa [10]	76 MPa [53]	0.30

Table 2: Properties of the base material of M130 foam.

3 FINITE ELEMENT MODEL SETUP

In the numerical models, cell walls were meshed with shell elements (S4R in Abaqus FE software). Abaqus/Explicit was utilised to perform numerical compressive and shear tests because it can model well cell wall buckling and contact. However, it should be stressed that Abaqus/Explicit is used here to study the quasi-static response of foams.

Two analytic rigid shells with a reference point attached with each were created and positioned at the top and bottom of the finite element models (Figure 1a). For compressive tests, the bottom rigid shell was fixed, and the top rigid shell was given a downward constant velocity. An element node which touches the bottom rigid shell was constrained from translational movement to prevent rigid body motion. In shear tests, the models were attached to the rigid shells at the interfaces using tie constraints. The bottom rigid shell was kept fixed and the top rigid shell was given a sidewise (along the x axis) constant velocity. The nodes on the side faces (face1 and face2 in Figure 1b) were constrained from moving vertically (along the y axis). With these constraints, a uniform shear strain field was generated in the finite element models.

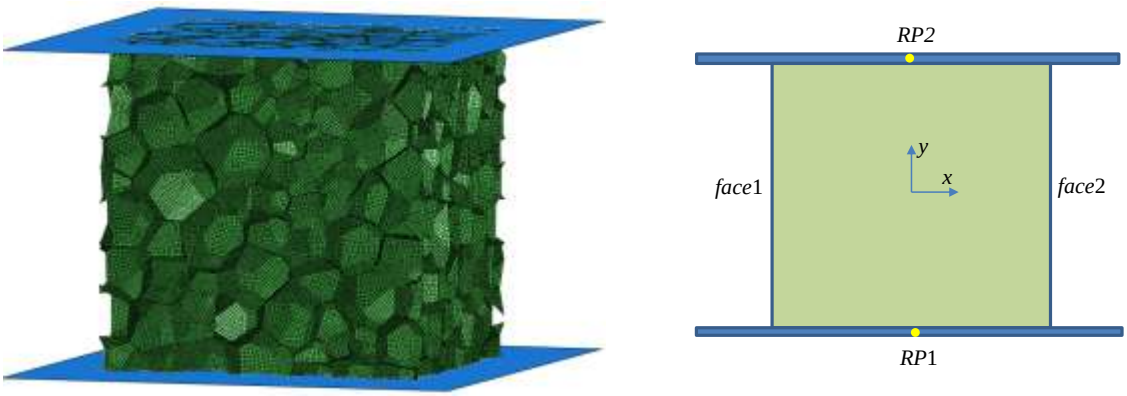

(a) (b)

Figure 1: (a) Laguerre model with two rigid shells attached; (b) schematics of Laguerre models and analytic rigid shells.

The density of the base material of the foam was increased 100 times in order to reduce the computational time [54]. General contact in Abaqus/Explicit with a friction coefficient of 0.2 was used. The majority of the models had around 200,000 nodes. All the simulations were run on a high-performance computer with two nodes (each with a 2.7 GHz processor) and with 16 GB memory. The solution time for each model was roughly 24 hours. The reaction force at the reference point RP1 (see Figure 1b) was obtained. Engineering stress (reaction force over the cross-sectional area of models) and strain (displacement of RP2 over the height of the models) were employed to describe the global response of the models. For the compressive tests, the first maximum global stress in the stress-strain

curves was taken as the compressive strength. For the shear tests, the 2% offset yield stress from the stress-strain curves was taken as the shear strength in the experimental study in [52] and therefore was chosen here as well. The shear stiffness was taken from our previous study [10].

4 SELECTION OF SIMULATION PARAMETERS

4.1 Loading rate

When an explicit solver is used to analyse a quasi-static process, a low loading rate needs to be selected in order to reduce the dynamic effects and approach a quasi-static condition. On the other hand, low loading rates increase the simulation time. Hence, different velocities applied on the top rigid shell were investigated. Figure 2 shows the ratio of the kinetic energy to the internal energy of the sample with different applied velocities in the compressive tests. The ratios are mostly below 5% for all these velocities, which implies the overall dynamic effect is negligible [54]. Since the computational time for these velocities are reasonable. The velocities 300 and 200 mm/s were selected for compressive and shear tests, respectively so as to obtain the stress-strain curves with the least dynamic effect.

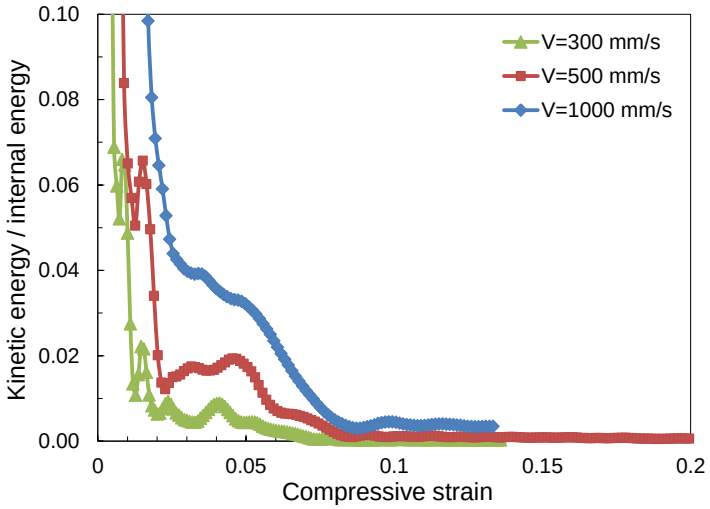

Figure 2: Variation of the ratio of kinetic energy to internal energy in compressive tests with different initial velocities.

4.2 Mesh sensitivity

To study the mesh density sensitivity and ensure mesh convergence, a sample (based on a random close packing of 1000 spheres) with the element sizes of 0.030, 0.0225 and 0.015 mm (termed meshes #1, #2 and #3) were tested under compression and shear. Figure 3 shows the variation of predicted compressive and shear strengths with element size. Considering the accuracy of results and the computational cost, an element size of 0.0225 mm (mesh #2) was chosen for further study.

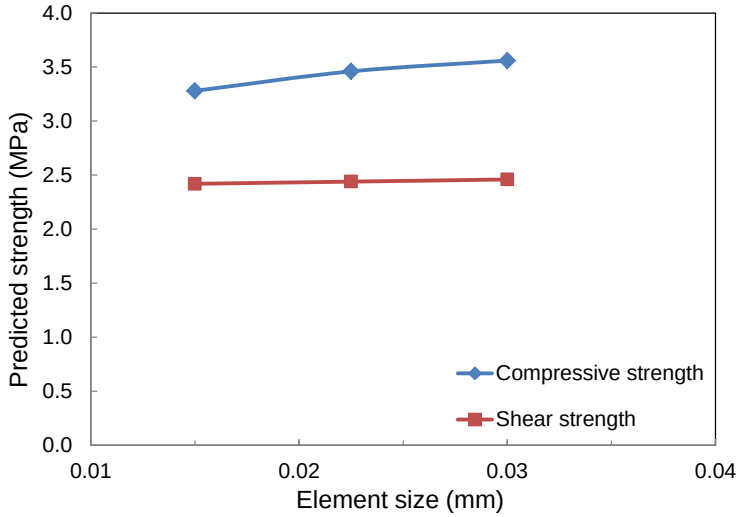

Figure 3: Variation of predicted compressive and shear strengths with element size.

4.3 Model size

Selection of model size is crucial in micromechanical modelling, as overly-large models could be highly computationally expensive, and overly-small models may not accurately represent the relevant material and structural features and thus may not yield accurate results. In the present study, Laguerre models based on random close packing of 1000, 1500 and 2000 spheres were considered. For each model size, three samples were tested. Figure 4 shows the predicted compressive and shear strengths with model size. It is noted that the difference in compressive and shear strengths predicted by these model sizes is minor. Considering the balance between the accuracy of results and the computational expense, the Laguerre models based on random close packing of 1500 spheres were employed in the further study.

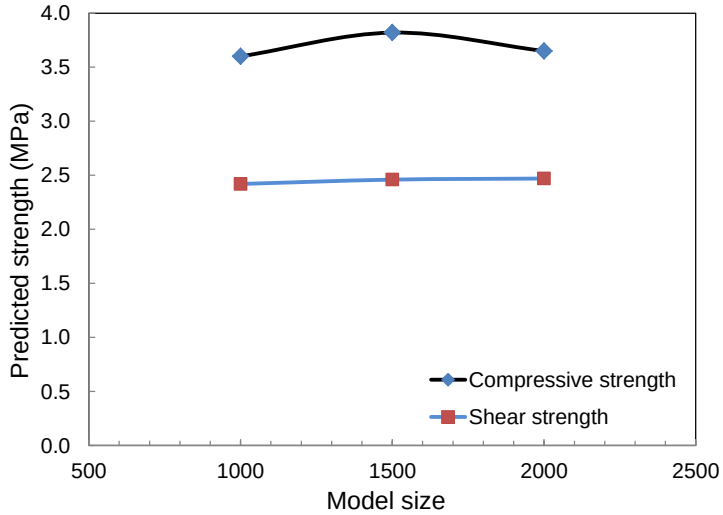

Figure 4: Variation of predicted compressive strength with model size.

5 RESULTS AND DISCUSSION

5.1 Effect of cell size variation on foam strength

The effect of cell size variation on foam strength is investigated in this section. To this end, five cell size distributions were considered. The cell size was assumed to vary according to a lognormal distribution. All the five distributions considered had the same average value but different standard deviations (see Table 3). The location and scale parameters of lognormal distributions are μ_1 and σ_1,

and σ_1 reflects the dispersion or variation of cell size. For each distribution, three samples were tested. To isolate the effect of cell size, the relative density of each sample was kept the same (0.1383), and the cell walls in each sample had the same thickness.

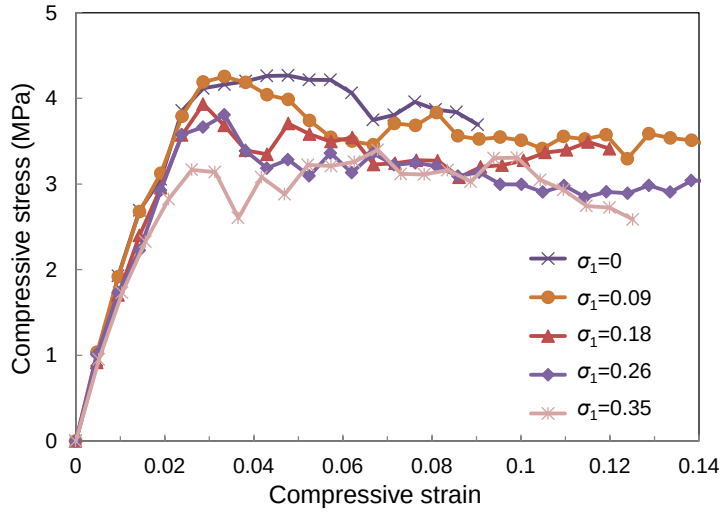

(a)

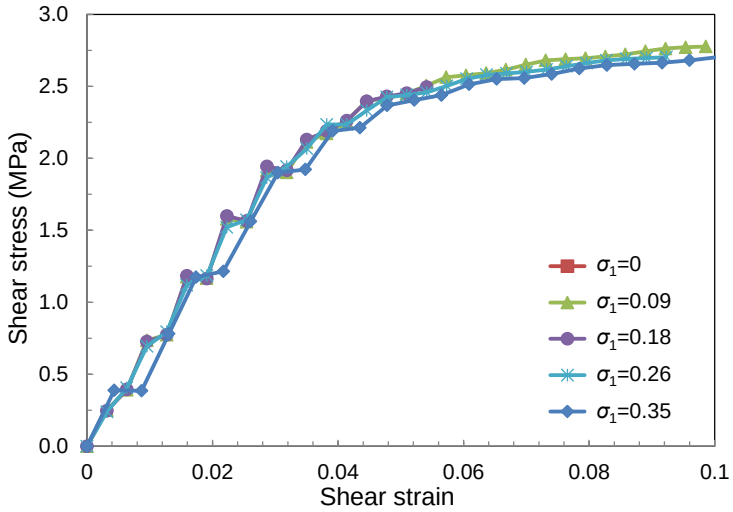

(b)

Figure 5: (a) Compressive and (b) shear stress-strain curves of samples with different cell size variations.

Figure 5 shows the compressive and shear stress-strain curves of some of these samples (one representative sample for each distribution). A considerable difference is noticed in the compressive stress-strain curves across these cell size variations; whist little difference is observed in the shear stress-strain curves. Table 3 lists the compressive and shear strengths of all these samples, and Figure 6 shows the variation of normalised compressive and shear strengths (by the respective strengths of samples with uniform cell size) with the cell size variation parameter (σ_1). It is found that the compressive strength decreases at an increasing rate as the cell size variation increases (by 25% when σ_1=0.3475). The shear strength remains constant initially but begins to decrease (by 6%) when the cell size dispersion parameter (σ_1) reaches a certain value (σ_1=0.3475). It is noted that the effect of cell size variation on compressive strength is more pronounced compared to shear strength. Comparing with the effect of cell size variation on stiffness found in our previous study [10], cell size variation reduces compressive strength more than compressive stiffness, i.e., by 25% for compressive strength and 9%

for compressive stiffness when σ_1=0.3475, whilst the reductions in shear stiffness and strength at a given cell size variation (σ_1) are rather close.

	μ_1	σ_1	Sample	Compressive strength (MPa)		Shear strength (MPa)	
				All	Average	All	Average
1	5.5452	0.0000	Sample #1	4.34	4.39	2.58	2.57
			Sample #2	4.55		2.57	
			Sample #3	4.27		2.56	
2	5.5412	0.0897	Sample #4	4.25	4.26	2.58	2.58
			Sample #5	4.31		2.60	
			Sample #6	4.23		2.57	
3	5.5293	0.1783	Sample #7	3.81	3.92	2.56	2.57
			Sample #8	3.93		2.56	
			Sample #9	4.03		2.59	
4	5.5101	0.2648	Sample #10	3.81	3.81	2.55	2.55
			Sample #11	3.71		2.59	
			Sample #12	3.92		2.50	
5	5.4853	0.3475	Sample #13	3.23	3.29	2.33	2.42
			Sample #14	3.17		2.51	
			Sample #15	3.48		2.43	

* μ_1 and σ_1 are the lognormal distribution parameters of cell size, with σ_1 reflecting the dispersion of cell size

Table 3: Compressive and shear strengths of samples with different cell size variations.

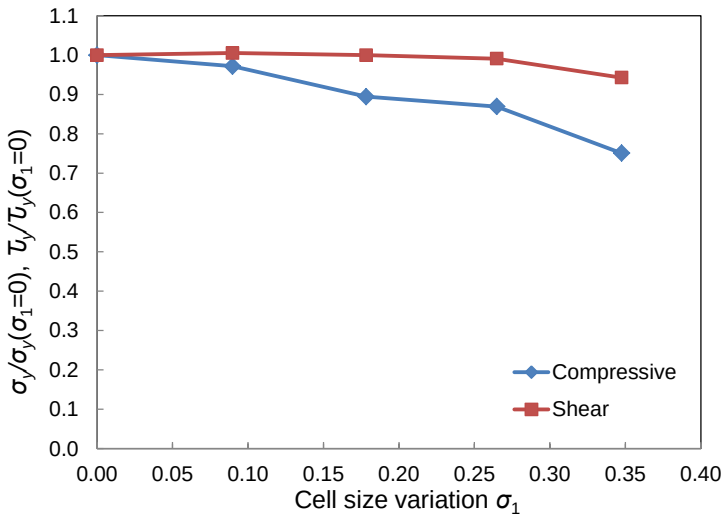

Figure 6: Variation of normalised compressive and shear strengths with cell size variation parameter.

5.2 Effect of wall thickness variation on foam strength

The effect of cell wall thickness variation on foam strength is studied in this section. To do so, Four cell wall thickness distributions were considered. The cell wall thickness was found to vary according to a lognormal distribution from measurements. All the four distributions considered had the same average value but different standard deviations (see Table 4). The location and scale parameters of lognormal distributions are denoted by μ_2 and σ_2, where σ_2 reflects the dispersion or variation of cell wall thickness. To consider the effect of cell wall thickness variation on the compressive and shear

strengths only and eliminate the effect of cell size variation, the structure of Sample #3 which has cells of uniform size was taken as a base, and the four cell wall thickness distributions were incorporated into it to generate various foam models with nearly the same mean cell wall thickness but different dispersions. The relative density of each sample was kept constant at 0.1383. Three samples were created and tested for each cell wall thickness distribution.

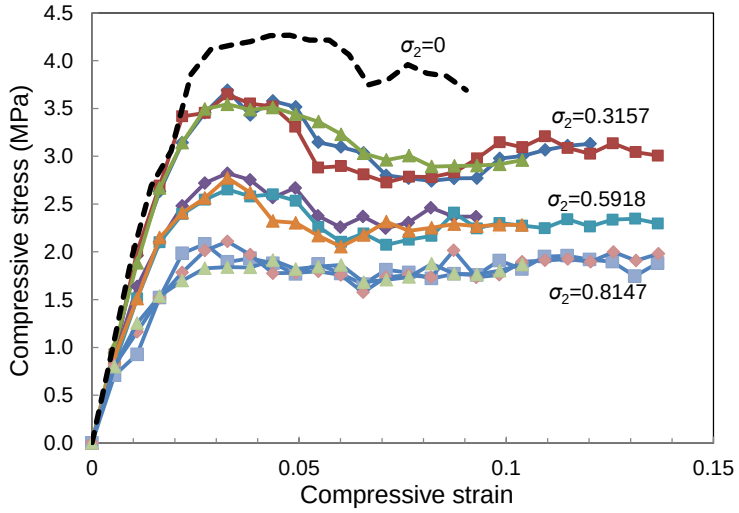

(a)

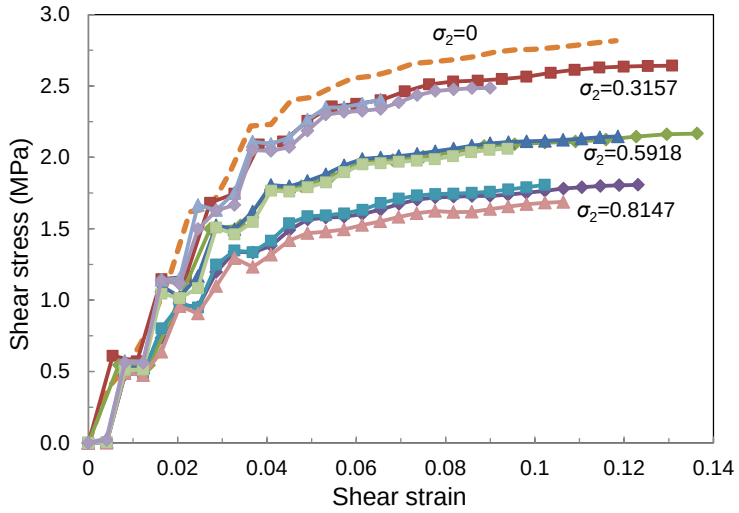

(b)

Figure 7: (a) Compressive and (b) shear stress-strain curves of samples with cells of uniform size but having non-uniform wall thickness.

Figure 7 shows the compressive and shear stress-strain curves of these samples. Considerable differences are shown in stress-strain curves across different cell wall thickness variations. Table 4 lists the compressive and shear strengths of these models, and Figure 8 shows the variations of normalized compressive and shear strengths with cell wall thickness variation parameter. It is noticeable that both the compressive and shear strengths decrease with cell wall thickness variation, and the compressive strength is reduced more than the shear strength at a given cell wall thickness variation. The effect of cell size variation on the compressive and shear strengths is comparable to that of cell wall thickness variation on them, i.e., the compressive strength reduces roughly by 20% if σ_1= 0.32 or σ_2 =0.32. However, in M130 foams, cell wall thickness is more dispersed than cell size ($\sigma_2 > \sigma_1$), and thus cell wall thickness variation is the main factor that causes the strengths of M130 foams to deviate from their ideal potential values (i.e., the strengths of foams with uniform cell size and cell wall thickness). Comparing with the effect of cell wall thickness variation on compressive and shear

stiffnesses (found in our previous paper [10]), the effect of cell wall thickness variation on compressive and shear strengths is more pronounced.

	μ_2	σ_2	Sample	Compressive strength (MPa)		Shear strength (MPa)	
				All	Average	All	Average
1	2.226	0.0000	Sample #3	4.27	4.27	2.56	2.56
2	2.176	0.3157	Sample #16	3.69	3.63	2.37	2.35
			Sample #17	3.65		2.37	
			Sample #18	3.54		2.32	
3	2.051	0.5918	Sample #19	2.82	2.75	1.87	1.90
			Sample #20	2.65		1.94	
			Sample #21	2.77		1.89	
4	1.8945	0.8147	Sample #22	2.08	2.03	1.60	1.55
			Sample #23	2.11		1.58	
			Sample #24	1.91		1.48	

*μ_2 and σ_2 are the lognormal distribution parameters of cell wall thickness, with σ_2 reflecting the dispersion of cell wall thickness.

Table 4: Compressive and shear strength of samples of samples with cells of uniform size but having non-uniform wall thickness

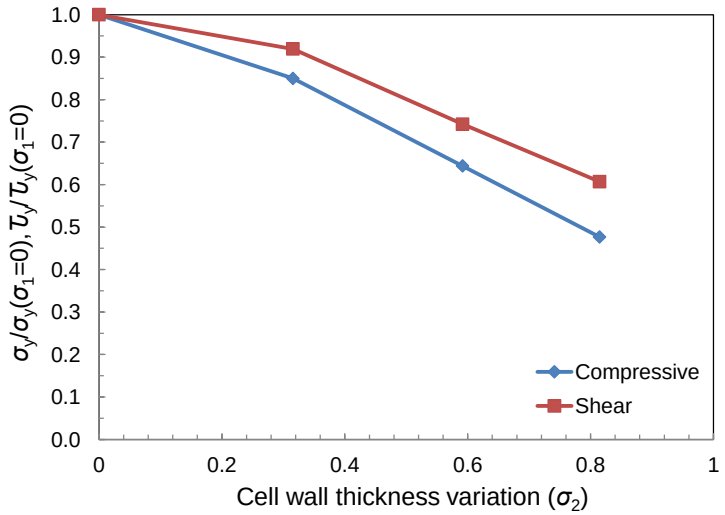

Figure 8: Variation of normalised compressive and shear strengths with cell wall thickness variation parameter.

5.3 Combined effect of cell size and cell wall thickness variations

In the previous two sections, the effects of cell size and cell wall thickness variations on foam strengths were investigated separately. The combined effect of cell wall thickness and cell size variations is studied in this section. To do so, the structures of Samples #15 and #14 which have a cell size variation parameter (σ1) of 0.3475 were used as base cases, and the four cell wall thickness distributions mentioned before in Section 6 were integrated with these structures. Three samples were created and tested for each cell wall thickness distribution.

Figure 9 shows the compressive and shear stress-strain curves of these samples. Likewise, considerable differences in the stress-strain curves were noted across these cell wall thickness variations. Table 5 lists the compressive and shear strengths of these samples, and Figure 10 shows the variations of normalised compressive and shear strengths (by the respective strengths of Samples #1-#3) with cell wall thickness variation parameter. It is noteworthy that strength reduction caused by cell wall thickness variation is less pronounced in foams with non-uniform cell size. This means that the

effect of cell wall thickness variation on the strength reduction of closed-cell foams is diminished by cell size variation.

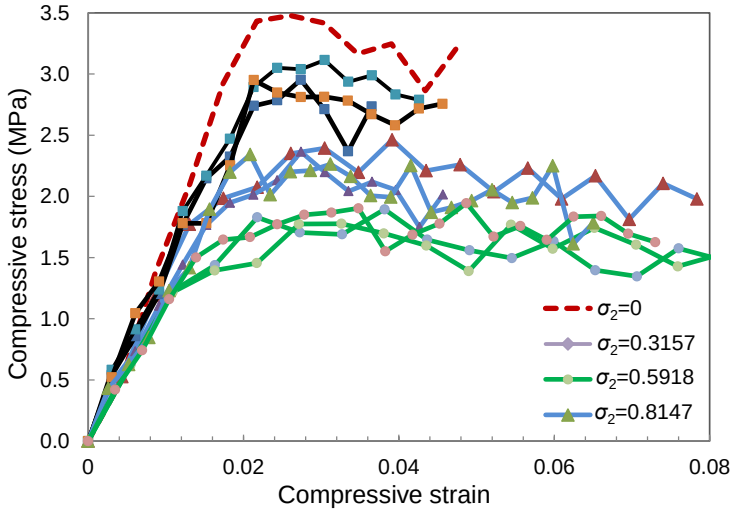

(a)

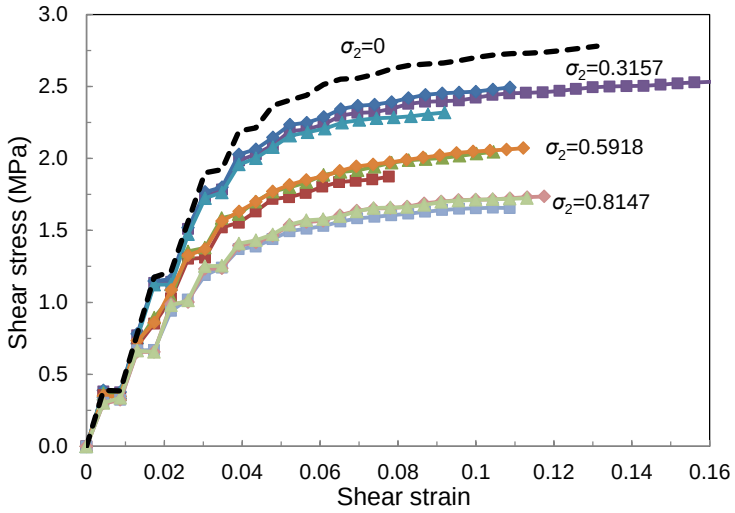

(b)

Figure 9: (a) Compressive and (b) shear stress-strain curves of samples with different cell size variations.

Samples #31-33, and #40-42 have the same relative density, cell size and cell wall thickness distributions as M130 foam. But, the compressive and shear strengths predicted by them (see Table 5) are about 20% lower than those of M130 foam as sourced from the datasheet (see Table 1). One of the reasons for this is that the relative density of the Laguerre modes was calculated by

$$R = \frac{\sum_{i=1}^{n} A_i t_i}{V} \tag{1}$$

where R is the relative density, A_i and t_i are the area and thickness, respectively, of a cell wall, V is the volume of Laguerre models. This calculation method ignores the overlapping of materials in cell wall junctions arising from the application of shell elements (see Figure 11). As a result, the actual relative density of the Laguerre models used is less than 0.1383. Determining the exact volume fraction of material overlapping in cell wall junctions is difficult. Assuming that the volume fraction of overlapping materials in the Laguerre models is approximately the same as that in the Kelvin closed-

cell foam, then the volume fraction of overlapping materials can be calculated using Eq. (10) in [2]. Using this equation, it is found that a Laguerre model with a nominal relative density (calculated by Eq.(1)) of 0.1453 has an actual relative density (calculated by Eq. (10) in [2]) of 0.1383. With a relative density of 0.1453, the compressive and shear strengths predicted by the Laguerre models are 2.10 and 1.65 MPa, respectively. Other reasons might be that the real yield strength of the base material of M130 foam might be larger than the value of 76 MPa used here; a few cell walls were curved in the models, or solid concentrated in Plateau borders might have increased foam strength.

	μ_2	σ_2	Sample	Compressive strength (MPa)		Sample	Shear strength (MPa)	
				All	Average		All	Average
1	2.226	0.0000	Sample #15	4.27	3.48	Sample #14	2.51	2.51
2	2.176	0.3157	Sample #25	2.95	2.98	Sample #34	2.23	2.23
			Sample #26	3.05		Sample #35	2.28	
			Sample #27	2.95		Sample #36	2.18	
3	2.051	0.5918	Sample #28	2.36	2.36	Sample #37	1.85	1.81
			Sample #29	2.39		Sample #38	1.83	
			Sample #30	2.34		Sample #39	1.76	
4	1.8945	0.8147	Sample #31	1.83	1.84	Sample #40	1.57	1.55
			Sample #32	1.90		Sample #41	1.56	
			Sample #33	1.78		Sample #42	1.51	

*μ_2 and σ_2 are the lognormal distribution parameters of cell wall thickness, with σ_2 reflecting the dispersion of cell wall thickness.

Table 5: Compressive and shear strength of samples with different cell size variations

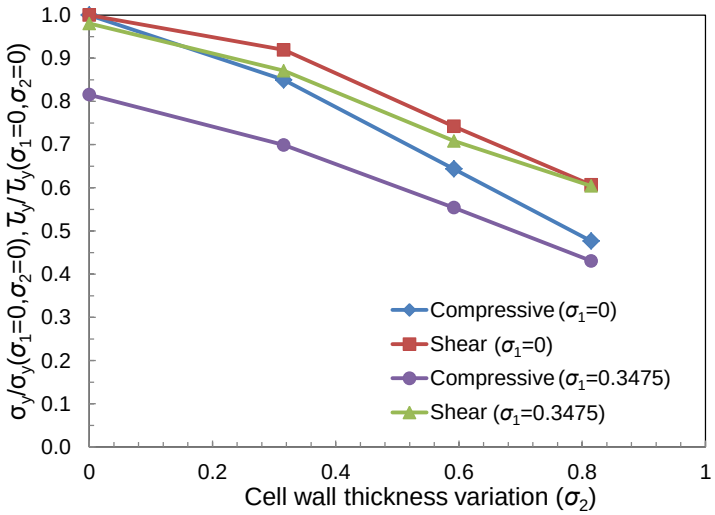

Figure 10: Variation of normalised compressive and shear strengths with cell wall thickness variation parameter

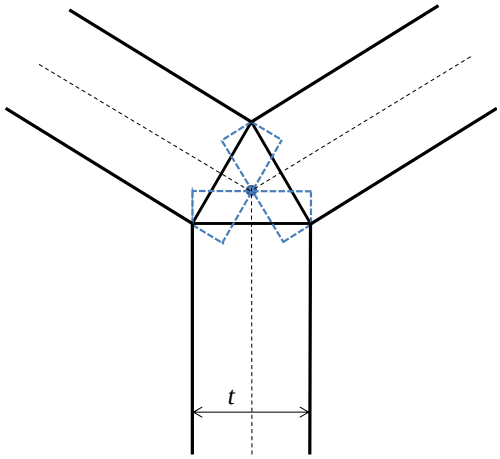

Figure 11: Schematic of overlapping of materials in cell wall junction.

9 CONCLUSIONS

In this work, the effects of cell size and cell wall thickness variations on the compressive and shear strengths of closed-cell foams were investigated using Laguerre tessellation models. It is found that compressive and shear strengths decrease as variability in cell size and cell wall thickness increase. Compressive strength is found to be more sensitive to these variations. The effect of cell size variation on compressive and shear strengths is comparable to that of cell wall thickness variation on them. However, in M130 foam cell wall thickness is more dispersed than cell size, and thus cell wall thickness variation is the main factor that causes the strengths of M130 foam to deviate from its ideal values. The combined effect of cell size and cell wall thickness variations on strengths is less than the sum of individual effect. Comparing to the effects on stiffness reduction, the effects of cell size and cell wall thickness variations on compressive and shear strengths reduction are more pronounced.

REFERENCES

[1] L. J. Gibson and M. F. Ashby, Cellular solids : structure and properties, 2nd ed. Cambridge ; New York: Cambridge University Press, 1997.

[2] A. Simone and L. Gibson, "Effects of solid distribution on the stiffness and strength of metallic foams," Acta Materialia, vol. 46, pp. 2139-2150, 1998.

[3] A. Simone and L. Gibson, "The effects of cell face curvature and corrugations on the stiffness and strength of metallic foams," Acta Materialia, vol. 46, pp. 3929-3935, 1998.

[4] J. L. Grenestedt and F. Bassinet, "Influence of cell wall thickness variations on elastic stiffness of closed-cell cellular solids," International Journal of Mechanical Sciences, vol. 42, pp. 1327-1338, 2000.

[5] W. Y. Jang, A. M. Kraynik, and S. Kyriakides, "On the microstructure of open-cell foams and its effect on elastic properties," International Journal of Solids and Structures, vol. 45, pp. 1845-1875, Apr 2008.

[6] M. Attia, S. Meguid, K. Tan, and S. Yeo, "Influence of cellular imperfections on mechanical response of metallic foams," International Journal of Crashworthiness, vol. 15, pp. 357-367, 2010.

[7] H. X. Zhu and A. H. Windle, "Effects of cell irregularity on the high strain compression of open-cell foams," Acta Materialia, vol. 50, pp. 1041-1052, 2002.

[8] C. Chen, T. J. Lu, and N. A. Fleck, "Effect of imperfections on the yielding of two-dimensional foams," Journal of the Mechanics and Physics of Solids, vol. 47, pp. 2235-2272, 1999.

[9] S. Ribeiro-Ayeh, "Finite element modelling of the mechanics of solid foam materials," Karlstad University, 2005.

[10] Y. Chen, R. Das, and M. Battley, "Effects of cell size and cell wall thickness variations on the stiffness of closed-cell foams," International Journal of Solids and Structures, 2014.

[11] C. Redenbach, I. Shklyar, and H. Andrä, "Laguerre tessellations for elastic stiffness simulations of closed foams with strongly varying cell sizes," International Journal of Engineering Science, vol. 50, pp. 70-78, 2012.

[12] S. Nammi, P. Myler, and G. Edwards, "Finite element analysis of closed-cell aluminium foam under quasi-static loading," Materials & Design, vol. 31, pp. 712-722, 2010.

[13] H. Zhu, J. Knott, and N. Mills, "Analysis of the elastic properties of open-cell foams with tetrakaidecahedral cells," Journal of the Mechanics and Physics of Solids, vol. 45, pp. 319-343, 1997.

[14] D. Weaire and R. Phelan, "A counter-example to Kelvin's conjecture on minimal surfaces," Philosophical Magazine Letters, vol. 69, pp. 107-110, 1994.

[15] H. X. Zhu, J. R. Hobdell, and A. H. Windle, "Effects of cell irregularity on the elastic properties of open-cell foams," Acta Materialia, vol. 48, pp. 4893-4900, 2000.

[16] K. Li, X. L. Gao, and G. Subhash, "Effects of cell shape and strut cross-sectional area variations on the elastic properties of three-dimensional open-cell foams," Journal of the Mechanics and Physics of Solids, vol. 54, pp. 783-806, 2006.

[17] Y. Song, Z. Wang, L. Zhao, and J. Luo, "Dynamic crushing behavior of 3D closed-cell foams based on Voronoi random model," Materials & Design, vol. 31, pp. 4281-4289, 2010.

[18] C. Redenbach, "Microstructure models for cellular materials," Computational Materials Science, vol. 44, pp. 1397-1407, 2009.

[19] C. Lautensack, "Fitting three-dimensional Laguerre tessellations to foam structures," Journal of Applied Statistics, vol. 35, pp. 985-995, 2008.

[20] M. Geißendörfer, A. Liebscher, C. Proppe, C. Redenbach, and D. Schwarzer, "Stochastic multiscale modeling of metal foams," Probabilistic Engineering Mechanics, vol. 37, pp. 132-137, 2014.

[21] E. Maire, F. Wattebled, J. Buffiere, and G. Peix, "Deformation of a Metallic Foam Studied by X-Ray Computed Tomography and Finite Element Calculations," Microstructural Investigation and Analysis, Volume 4, pp. 68-73, 2006.

[22] C. Lin, K. Natesaiyer, and J. D. Miller, "High resolution X-ray microtomography based micro finite element analysis of mechanical properties of cellular material," in International Society for Industrial Process Tomography, 2014.

[23] S. H. Kim, H. J. Chung, and K. Y. Rhee, "Numerical Analysis on the Compressive Behaviors of Aluminum Foam Material Using Computed Tomography Imaging," Advanced Materials Research, vol. 123, pp. 567-570, 2010.

[24] Y. Sun, T. Lowe, S. McDonald, Q. Li, and P. Withers, "In Situ Investigation and Image-Based Modelling of Aluminium Foam Compression Using Micro X-Ray Computed Tomography," in Visual Computing, ed: Springer, 2014, pp. 189-197.

[25] O. Caty, E. Maire, S. Youssef, and R. Bouchet, "Modeling the properties of closed-cell cellular materials from tomography images using finite shell elements," Acta Materialia, vol. 56, pp. 5524-5534, 2008.

[26] D. Ulrich, B. van Rietbergen, H. Weinans, and P. Rüegsegger, "Finite element analysis of trabecular bone structure: a comparison of image-based meshing techniques," Journal of Biomechanics, vol. 31, pp. 1187-1192, 1998.

[27] M. Vesenjak, C. Veyhl, and T. Fiedler, "Analysis of anisotropy and strain rate sensitivity of open-cell metal foam," Materials Science and Engineering: A, vol. 541, pp. 105-109, 2012.

[28] B. Notarberardino, "Image based finite element modelling for the mechanical characterisation of complex material systems," 2010.

[29] S. Youssef, E. Maire, and R. Gaertner, "Finite element modelling of the actual structure of cellular materials determined by X-ray tomography," Acta Materialia, vol. 53, pp. 719-730, 2005.

[30] J. Wismans, L. Govaert, and J. Van Dommelen, "X-ray computed tomography-based modeling of polymeric foams: The effect of finite element model size on the large strain response," Journal of Polymer Science Part B: Polymer Physics, vol. 48, pp. 1526-1534, 2010.

[31] Y. Sun, Q. Li, T. Lowe, S. McDonald, and P. Withers, "Investigation of strain-rate effect on the compressive behaviour of closed-cell aluminium foam by 3D image-based modelling," Materials & Design, vol. 89, pp. 215-224, 2016.

[32] R. Huang, P. Li, and T. Liu, "X-ray microtomography and finite element modelling of compressive failure mechanism in cenosphere epoxy syntactic foams," Composite Structures, vol. 140, pp. 157-165, 2016.

[33] I. Jeon, T. Asahina, K.-J. Kang, S. Im, and T. J. Lu, "Finite element simulation of the plastic collapse of closed-cell aluminum foams with X-ray computed tomography," Mechanics of Materials, vol. 42, pp. 227-236, 2010.

[34] N. Daphalapurkar, J. Hanan, N. Phelps, H. Bale, and H. Lu, "Tomography and simulation of microstructure evolution of a closed-cell polymer foam in compression," Mechanics of Advanced Materials and Structures, vol. 15, pp. 594-611, 2008.

[35] C. Petit, S. Meille, and E. Maire, "Cellular solids studied by x-ray tomography and finite element modeling–a review," Journal of Materials Research, vol. 28, pp. 2191-2201, 2013.

[36] L. Zhang, J. M. Ferreira, S. Olhero, L. Courtois, T. Zhang, E. Maire, and J. C. Rauhe, "Modeling the mechanical properties of optimally processed cordierite–mullite–alumina ceramic foams by X-ray computed tomography and finite element analysis," Acta Materialia, vol. 60, pp. 4235-4246, 2012.

[37] A. Burteau, F. N'Guyen, J. D. Bartout, S. Forest, Y. Bienvenu, S. Saberi, and D. Naumann, "Impact of material processing and deformation on cell morphology and mechanical behavior of polyurethane and nickel foams," International Journal of Solids and Structures, vol. 49, pp. 2714-2732, Oct 1 2012.

[38] E. B. Matzke, "The three-dimensional shape of bubbles in foam-an analysis of the rôle of surface forces in three-dimensional cell shape determination," American Journal of Botany, pp. 58-80, 1946.

[39] J. Köll and S. Hallström, "Morphology effects on constitutive properties of foams," presented at the 18th International conference on composite materials, Jeju Island, South Korea, 2011.

[40] Z. Fan, Y. Wu, X. Zhao, and Y. Lu, "Simulation of polycrystalline structure with Voronoi diagram in Laguerre geometry based on random closed packing of spheres," Computational Materials Science, vol. 29, pp. 301-308, 2004.

[41] S. Kanaun and O. Tkachenko, "Mechanical properties of open cell foams: Simulations by Laguerre tesselation procedure," International Journal of Fracture, vol. 140, pp. 305-312, 2006.

[42] A. M. Kraynik, D. A. Reinelt, and F. van Swol, "Structure of random foam," Physical Review Letters, vol. 93, Nov 12 2004.

[43] H. Zhu, P. Zhang, D. Balint, S. Thorpe, J. Elliott, A. Windle, and J. Lin, "The effects of regularity on the geometrical properties of Voronoi tessellations," Physica A: Statistical Mechanics and its Applications, vol. 406, pp. 42-58, 2014.

[44] H. X. Zhu, S. M. Thorpe, and A. H. Windle, "The effect of cell irregularity on the high strain compression of 2D Voronoi honeycombs," International Journal of Solids and Structures, vol. 43, pp. 1061-1078, 2006.

[45] A. P. Roberts and E. J. Garboczi, "Elastic moduli of model random three-dimensional closed-cell cellular solids," Acta Materialia, vol. 49, pp. 189-197, 2001.

[46] N. Mills and H. Zhu, "The high strain compression of closed-cell polymer foams," Journal of the Mechanics and Physics of Solids, vol. 47, pp. 669-695, 1999.

[47] N. Mills, R. Stämpfli, F. Marone, and P. Brühwiler, "Finite element micromechanics model of impact compression of closed-cell polymer foams," International Journal of Solids and Structures, vol. 46, pp. 677-697, 2009.

[48] H. Bart-Smith, A. F. Bastawros, D. Mumm, A. Evans, D. Sypeck, and H. Wadley, "Compressive deformation and yielding mechanisms in cellular Al alloys determined using X-ray tomography and surface strain mapping," Acta Materialia, vol. 46, pp. 3583-3592, 1998.

[49] A.-H. Benouali, L. Froyen, T. Dillard, S. Forest, and F. N'guyen, "Investigation on the influence of cell shape anisotropy on the mechanical performance of closed cell aluminium foams using micro-computed tomography," Journal of Materials Science, vol. 40, pp. 5801-5811, 2005.

[50] K. Li, X.-L. Gao, and A. Roy, "Micromechanics model for three-dimensional open-cell foams using a tetrakaidecahedral unit cell and Castigliano's second theorem," Composites Science and Technology, vol. 63, pp. 1769-1781, 2003.

[51] L. Gurit. (2016). Structural core materials. Available: http://www.gurit.com/structural-cores.aspx

[52] C. Alison, "Characterization of polymeric foam core materials," Master Thesis, The Department of Mechanical, The University of Auckland, New Zealand, 2012.

[53] M. Kutz, Mechanical engineers' handbook: John Wiley & Sons Inc, 2006.

[54] A. U. s. Manual, "Version 6.13," ABAQUS Inc, 2013.